www.czasopisma.pan.pl PAN POLSKA AKADEMIA NAUK www.journals.pan.pl

Archives of Acoustics Vol. 49, No. 1, pp. 83–93 (2024), doi: 10.24425/aoa.2023.146811

Research Paper

Normal Mode Solutions of Target Strengths of Solid-filled Spherical Shells and Discussion of Influence Parameters

Bing JIA[(1),(2)], Jun FAN[(1)*], Gui-Juan LI[(2)], Bin WANG[(1)], Yun-Fei CHEN[(2)]

[(1)] *Key Laboratory of Marine Intelligent Equipment and System Ministry of Education*
Shanghai Jiao Tong University
Shanghai, China

[(2)] *Science and Technology on Underwater Test and Control Laboratory*
Dalian, Liaoning, China

*Corresponding Author e-mail: fanjun@sjtu.edu.cn

(*received December 16, 2022; accepted April 5, 2023; published online October 2, 2023*)

The normal mode solution for the form function and target strength (TS) of a solid-filled spherical shell is derived. The calculation results of the spherical shell's acoustic TS are in good agreement with the results of the finite element method (FEM). Based on these normal mode solutions, the influences of parameters such as the material, radius, and thickness of the inner and outer shells on the TS of a solid-filled spherical shell are analyzed. An underwater spherical shell scatterer is designed, which uses room temperature vulcanized (RTV) silicone rubber as a solid filling material and does not contain a suspension structure inside. The scatterer has a good TS enhancement effect.

Keywords: solid-filled spherical shell; room temperature vulcanized silicone rubber; target strength enhancement.

1. Introduction

In underwater acoustic engineering, spherical acoustic scatterers have good directivity and are often used as standard test objects for the calibration of underwater active acoustic testing systems (Anstee, 2002; Foote *et al.*, 2007; Stanton, Chu, 2008; Islas-Cital, Atkins, 2012; Atkins *et al.*, 2017). The acoustic target strength (TS) represents the reflection ability of underwater targets with respect to acoustic waves. When the TS is larger, the target can be detected more easily by active sonar systems. To obtain a larger TS, spherical acoustic scatterers with geometric scattering as the primary mechanism are usually large in volume and mass, resulting in challenges for offshore deployment. Therefore, the current research focuses on the design of TS enhancement of spherical scatterers with constant volume, including the design of medium frequency thickness resonance (Xu *et al.*, 2020) and acoustic focusing. In recent years, the calibration of liquid-filled focusing spheres as standard scatterers has also been applied in some scenarios (Deveau, Lyons, 2009; Foote, 2018). Research on focusing spheres, which are thin spherical shells filled with liquids, has been carried out on the focusing effects of different filling liquids (Jia *et al.*, 2020). However, since the material CCL4 (carbon tetrachloride) commonly used in liquid-filled spheres is toxic and the focusing effect is affected by external water temperature (Deng *et al.*, 1982), studying solid-filled spherical shells with the TS enhancement effect becomes crucial and meaningful. Similar to the focusing effect of liquid, solid fillers that meet certain sound velocity and density conditions should also have a focusing effect to enhance TS, which needs further research.

In the construction process of underwater spherical acoustic scatterers, to meet certain TS design requirements, it is necessary to establish a calculation method and discuss the influence of the spherical shell diameter, thickness, material, and acoustic characteristics of filling materials on the TS. In the earliest research on spherical sound scatterers, a common assumption

was that the scatterer was a rigid material, and an approximate solution was proposed in which the wavelength was larger than the spherical diameter scattering sound field. Then, the normal series solution of a thin shell filled with air was studied (Junger, 1952; Goodman, Stern, 1962). With the demand for spherical targets with small volume and large TS, researchers have studied liquid-filled spherical shells with a certain focusing effect, obtained the normal series solution of spherical acoustic scatterers placed in water, further analyzed the relationship between the parameters of the liquid as the filling material and TS, and carried out experimental verifications (Kaduchak, Loeffler, 1998; Fawcett, 2001). In addition, researchers have theoretically derived the analytical solution of the double-layer elastic spherical shell in water (Tang, Fan, 1999), and researched the echo characteristics of the double-layer elastic spherical shell in the case of equivalent laying layers (Fan, Tang, 2001; Tang *et al.*, 2018). The derivation process and condition settings provide important inspiration for the theoretical derivation of other spherical shells. In addition, the impact of an elastic sphere composed of new materials on TS was studied (Zhou *et al.*, 2019; 2020).

In this paper, the method of separating variables is used to derive the normal mode solutions of the TS of a solid-filled spherical shell. Based on the normal mode solution, the far field form function of the echo of the spherical shell is calculated. We also discuss the influence of the outer spherical shell material, thickness, acoustic characteristics of the inner solid-filled material, and radius on the TS of the spherical shell. Finally, the feasibility of the specific RTV material as the filling material is discussed, which provides theoretical support for the design of the solid-filled spherical shell.

2. Normal mode solution of the scattering sound field from a solid-filled spherical shell

The problem of sound scattering from a solid-filled spherical shell can be simplified as the solution of the sound field of sound propagating in a four-layered medium, as shown in Fig. 1a. The areas (1), (2), (3), (4) are marked. Each area represents one of the four-layered media. Area (1) is the surrounding medium of water in which the spherical shell is located. Area (2) is a spherical shell. Area (3) is the interlayer between the solid core and the spherical shell. Area (4) is a solid core and, in this study, RTV material is used as the solid filling material. Figure 1b illustrates acoustic focusing in multilayer targets, the scattered wave consists of an elastic wave and a focused wave, and the incident plane waves converge on the spherical shell and reflect.

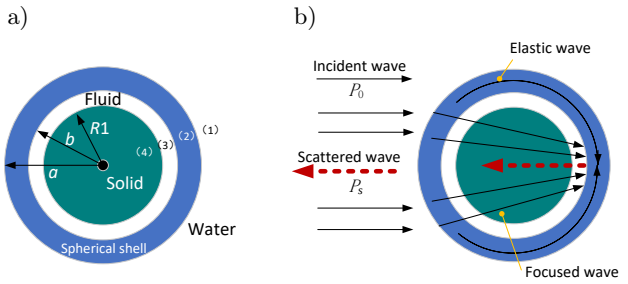

Fig. 1. Structure and focusing phenomenology of a solid-filled spherical shell: a) structure of a solid-filled spherical shell; b) acoustic focusing in multilayer targets.

In underwater acoustics, form function $f(x,\theta)$ is commonly used to describe the far-field scattering characteristics of targets:

$$f(x,\theta) = \frac{2r}{a}\frac{P_s(x,\theta)}{P_0(x)}e^{-ikr}, \tag{1}$$

where P_0 is the incident pressure, P_s is the scattered pressure, r is the distance, a is the size of the scatterer, $x = ka$ – is the dimensionless frequency, k is the wave number, and θ is the scattering angle.

The acoustic TS represents the backscattering ability of the target, and its relationship to the form function:

$$\mathrm{TS} = 10\log\left|\frac{a}{2}f(x,\pi)\right|^2, \tag{2}$$

where TS is the target strength.

When a steady plane wave is incident, the sound pressure can be expressed as:

$$P_0 = p_0\sum_{n=0}^{\infty} i^n(2n+1)j_n(k_1r)P_n(\cos\theta). \tag{3}$$

In the formula, the amplitude of the incident sound pressure p_0 is 1. We omit the time factor $e^{-j\omega t}$ both here and below.

The outer layer is water, the range is $r > a$, and only the compressional wave propagates. The total sound pressure of the outer sound field is:

$$P_1 = p_0\sum_{n=0}^{\infty} i^n(2n+1) \cdot \left[j_n(k_1r) + b_nh_n^{(1)}(k_1r)\right]P_n(\cos\theta). \tag{4}$$

The scalar potential $\boldsymbol{\Phi}$ is used in fluid, and scalar potential $\boldsymbol{\Phi}$ and vector potential $\boldsymbol{\varphi}$ (considering symmetry, only the component in the P_0 direction) are used in the elastic body to express the sound field.

The second layer is a solid spherical shell, and the range is $b < r < a$, including the compressional wave and shear wave.

The compressional wave field in a spherical shell is expressed as follows:

$$\boldsymbol{\Phi}_2 = p_0\sum_{n=0}^{\infty} i^n(2n+1) \cdot \left[c_nj_n(k_{d2}r) + d_ny_n(k_{d2}r)\right]P_n(\cos\theta). \tag{5}$$

Similarly, the shear wave field in a spherical shell is expressed as:

$$\boldsymbol{\varphi}_2 = p_0 \sum_{n=0}^{\infty} i^n (2n+1) \cdot [e_n j_n(k_{s2} r) + f_n y_n(k_{s2} r)] P_n(\cos\theta). \quad (6)$$

The third layer (middle layer) is the fluid layer, with the range of $R1 < r < b$ and only compressional waves:

$$p_3 = p_0 \sum_{n=0}^{\infty} i^n (2n+1) \cdot [g_n j_n(k_3 r) + q_n y_n(k_3 r)] P_n(\cos\theta). \quad (7)$$

The fourth layer is a solid sphere with the range $r < R1$, including the compressional wave and shear wave.

The compressional wave field in the fourth layer of the solid sphere is as follows:

$$\boldsymbol{\Phi}_4 = p_0 \sum_{n=0}^{\infty} i^n (2n+1) s_n j_n(k_{d4} r) P_n(\cos\theta). \quad (8)$$

The shear wave field in the fourth layer of the solid sphere is:

$$\boldsymbol{\varphi}_4 = p_0 \sum_{n=0}^{\infty} i^n (2n+1) u_n j_n(k_{s4} r) P_n(\cos\theta). \quad (9)$$

In Eqs. (4)–(9), n is the order, $j_n(X)$ is the n-th-order Bessel function, $y_n(X)$ is the n-th-order Neumann function, $h_n^{(1)}(X)$ is the n-th-order Hankel function of the first kind, and $P_n(X)$ is the n-th-order associated Legendre function.

Mentioned k_1 is the wavenumber of the outer water, k_{d2} is the compressional wavenumber of the second layer, and k_{s2} is the shear wavenumber of the second layer, k_3 is the wavenumber of the fluid medium in the middle layer, k_{d4} is the compressional wavenumber of the fourth layer's solid sphere, and k_{s4} is the shear wavenumber of this solid sphere.

In addition, b_n, c_n, d_n, e_n, f_n, g_n, q_n, s_n, and u_n are the undetermined coefficients.

There are nine boundary conditions:

$$T_{rr}^{(2)}|_{r=a} = -p_1, \quad u_r^{(1)}|_{r=a} = u_r^{(2)}|_{r=a}, \quad T_{r\theta}^{(2)}|_{r=a} = 0,$$

$$T_{rr}^{(2)}|_{r=b} = -p_3, \quad u_r^{(2)}|_{r=b} = u_r^{(3)}|_{r=b}, \quad T_{r\theta}^{(2)}|_{r=b} = 0,$$

$$T_{rr}^{(4)}|_{r=R1} = -p_3, \quad u_r^{(3)}|_{r=R1} = u_r^{(4)}|_{r=R1}, \quad T_{r\theta}^{(4)}|_{r=R1} = 0,$$

where $T_{rr}^{(2)}$ is the normal stress of the (2) layer boundary, $u_r^{(1)}$ is the displacement of the (1) layer boundary, and $T_{r\theta}^{(2)}$ is the tangential stress of the (2) layer boundary.

The undetermined coefficient b_n can be solved according to the following formal solution and boundary conditions:

$$b_n = -B_n/D_n, \quad (10)$$

where B_n and D_n are presented in Appendix.

The expression of the far-field form function of the backscattering of a solid-filled spherical shell is:

$$|f(k_1 a, \pi)| = \frac{2}{k_1 a} \left| \sum_{n=0}^{\infty} (-1)^n (2n+1) b_n \right|. \quad (11)$$

Accordingly, the expression of the spherical shell TS is:

$$\mathrm{TS} = 10 \log \left| \frac{a}{2} f(k_1 a, \pi) \right|^2. \quad (12)$$

3. Comparison between the normal mode and numerical solutions

To verify the normal mode solution derived above, the calculation results, using COMSOL Multiphysics version 5.5 – a common numerical calculation tool, are compared with the results of the normal mode solution. The numerical calculation tool uses the finite element method (FEM). Mesh size is selected as 1/6 of the wavelength corresponding to the highest frequency. The calculation conditions are as follows: the outer layer of the spherical shell is water, the spherical shell is steel with a radius of 1 m and a thickness of 0.1 m, the middle fluid layer is water, and the inner solid filler is a steel sphere with a radius of 0.8 m. See Table 1 for the specific parameter selection.

Table 1. Parameters of materials used in the paper.

Material	Density [kg/m^3]	Compressional wave velocity [m/s]	Shear wave velocity [m/s]
Water	1000	1482	–
Air	1.02	344	–
Aluminum	2700	6420	3040
Steel	7900	5940	3100
RTV (SDL-1-41)	1031	1030	202

Equation (11) involves the calculation of infinite series; according to (Tang *et al.*, 2018), the accuracy of the above infinite series can be guaranteed as long as the highest number of terms $n > ka+5$ is taken; ka is the non-dimensional frequency, k is the wavenumber, and a is the radius. In the calculation process, speed and accuracy are comprehensively considered. The order n is $ka + 20$, where ka is the non-dimensional frequency and the product of wavenumber k and target apparent scale a. Figure 2 shows the comparison results between the normal mode solution and the numerical solution. It can be seen that in the range of $ka < 30$, the normal mode solution and the finite element numerical solution are in good agreement overall. When ka is small

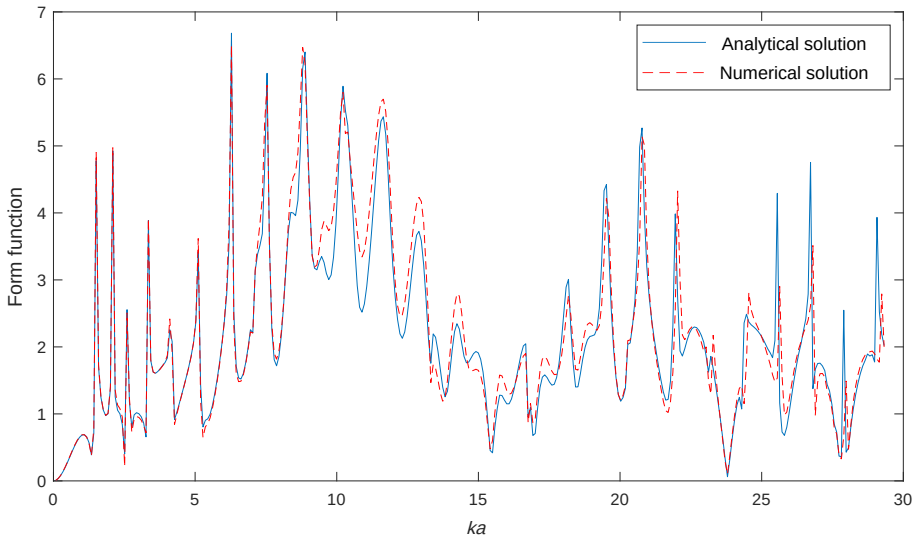

Fig. 2. Comparison of the normal mode solution and the numerical solution.

($ka < 10$ with the same size target and low frequency), the two solutions are completely consistent. In the case of large ka ($ka > 10$ with the same size target and high frequency), the peak position and trend of the morphological function calculated by the two methods are consistent. However, there are differences in the individual peak amplitudes, mainly because the grid size of the finite element calculation is limited after the frequency increases. Figure 2 can prove the accuracy of the normal mode solution derived in this paper, which provides a theoretical basis for the property analysis of the TS of the solid-filled spherical shell discussed next.

4. Analysis of the influencing factors on the TS of a solid-filled spherical shell in water

According to the structural characteristics of the solid-filled spherical shell, the main factors affecting the TS include the diameter, thickness and material of the spherical shell, the material of the middle layer, and the radius and material of the fourth layer of the solid sphere. The conclusion, "the larger the radius of the spherical shell, the stronger the TS", has been reached in classical underwater acoustics books and will not be analyzed here. In the following, we first discuss the material and thickness of the spherical shell, and then we select the material of the middle layer. Finally, we analyze and select the solid-filled material and the radius of the fourth layer solid sphere, and discuss the impact on the TS.

In the comparative analysis, the TS of a rigid sphere with the same radius is taken as the standard, and the calculation formula for the TS of a rigid sphere is:

$$\mathrm{TS} = 10 \log \frac{a^2}{4}, \tag{13}$$

where a is the radius of this sphere.

The applicable condition of Eq. (13) is $ka \gg 1$. In general, if the geometric optical zone of the rigid sphere is satisfied ($ka > 2\pi$), Eq. (13) can be used to estimate its TS.

4.1. Selection and analysis of the material and thickness of the spherical shell

In underwater acoustics, when spherical acoustic scatterers are used as underwater targets, common materials with reasonable costs include aluminum and steel. In addition, spherical acoustic scatterers made from the same material and diameter but with different shell thicknesses will also affect the TS of the spherical acoustic scatterers. This paper simulates the TS of an aluminum spherical shell and a steel spherical shell and obtains the comparison results (see Figs. 3–6). In our calculations, the shell material is aluminum or steel, the radius of the shell is 1 m, the ratio of the shell thick-

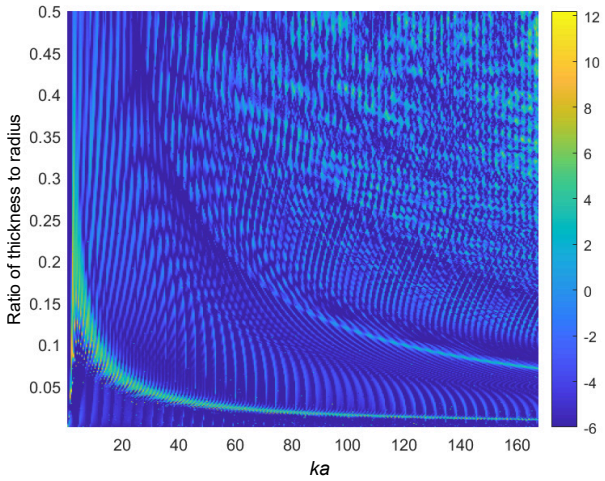

Fig. 3. TS of the aluminum spherical shell containing air varying with the thickness to radius ratio.

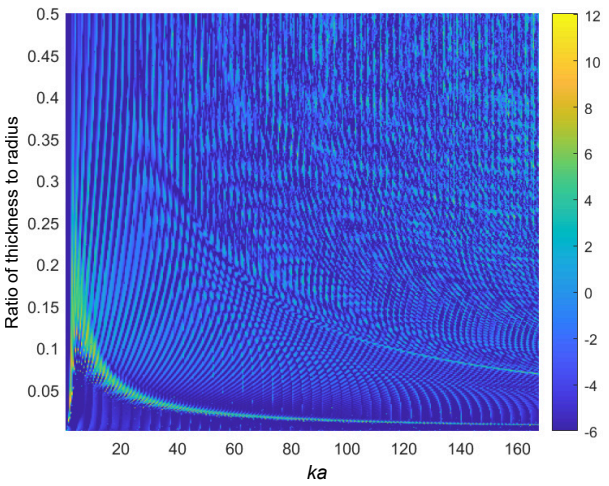

Fig. 4. TS of the steel spherical shell containing air varying with the thickness to radius ratio.

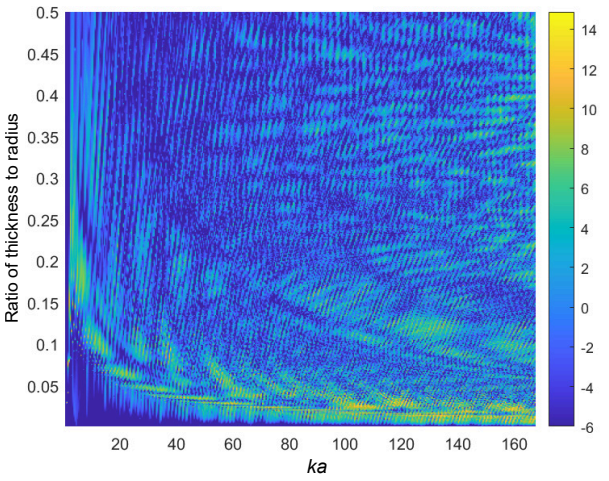

Fig. 5. TS of the aluminum spherical shell containing water varying with the thickness to radius ratio.

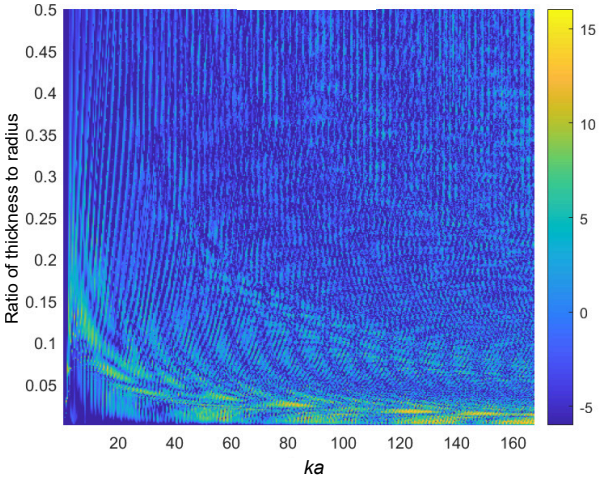

Fig. 6. TS of the steel spherical shell containing water varying with the thickness to radius ratio

ness to the radius is 0.1–50%, the step size is 0.1%, and the inner layer is air or water. Other material properties are shown in Table 1.

Figures 3 to 6 illustrate the four conditions of an air-filled aluminum spherical shell, an air-filled steel spherical shell, a water-filled aluminum spherical shell, and a water-filled steel spherical shell, respectively. Due to the existence of resonance under these conditions and with the gradual increase in the thickness to radius ratio, the maximum value of the TS moves to the small *ka*, that is, to the low frequency. However, when the thickness reaches a certain level (in this calculation, the ratio of thickness to radius of the aluminum shell is greater than 0.3, and the ratio of thickness to radius of the steel shell is greater than 0.25), the peak value of the TS disappears. It can be seen from the comparison between Fig. 4 and Fig. 6 that the main peak value of the air-filled structure is more obvious than that of the water-filled structure. Because the acoustic parameters of the air in the sphere and the water outside the spherical shell differ greatly, the sound field distribution is simpler than that of the water-filled structure. It can be seen from the TS color scale that the maximum TS of the water-filled structure is larger than that of the air-filled structure. The TS of the water-filled steel spherical shell is slightly higher than that of the water-filled aluminum spherical shell. Both steel and aluminum can be used as solid-filled spherical shells. In engineering design and processing, the shell material can be selected by comprehensively considering the processing difficulty, project cost, placement, and storage conditions.

To analyze the influence of the thickness of the solid spherical shell on the TS, the spherical shell is filled entirely with air, and the typical TS values of the spherical shell with different thickness to radius ratios are selected for comparison. The calculation results are shown in Fig. 7. The calculation conditions are as follows: the radius of the spherical shell is 1 m, the material is steel or aluminum, the spherical shell is filled with air, and the material outside the spherical shell is water. Other parameters are listed in Table 1.

When the ratio of shell thickness to radius is 1% (Figs. 7a and 7b) and *ka* is between 119 and 138, the steel spherical shell will exhibit resonance, and the TS can be increased by more than 6 dB. If *ka* is between 150 and 170, the aluminum spherical shell will resonate. With the increase in the thickness to radius ratio, the enhancement effect gradually moves to low frequency. When the ratio of thickness to radius is 2% (Figs. 7c and 7d) and *ka* is between 55 and 67, the steel spherical shell will resonate, and when *ka* is between 63 and 81, the aluminum spherical shell will resonate. When the thickness to radius ratio is 10% (Figs. 7e and 7f) and *ka* is between 5 and 11, the steel spherical shell will resonate, and if *ka* is between 6 and 14, the aluminum spherical shell will resonate.

By comparing the TS of the steel spherical shell and aluminum spherical shell with the *ka* change curve, it can be seen that the values of *ka* corresponding to the

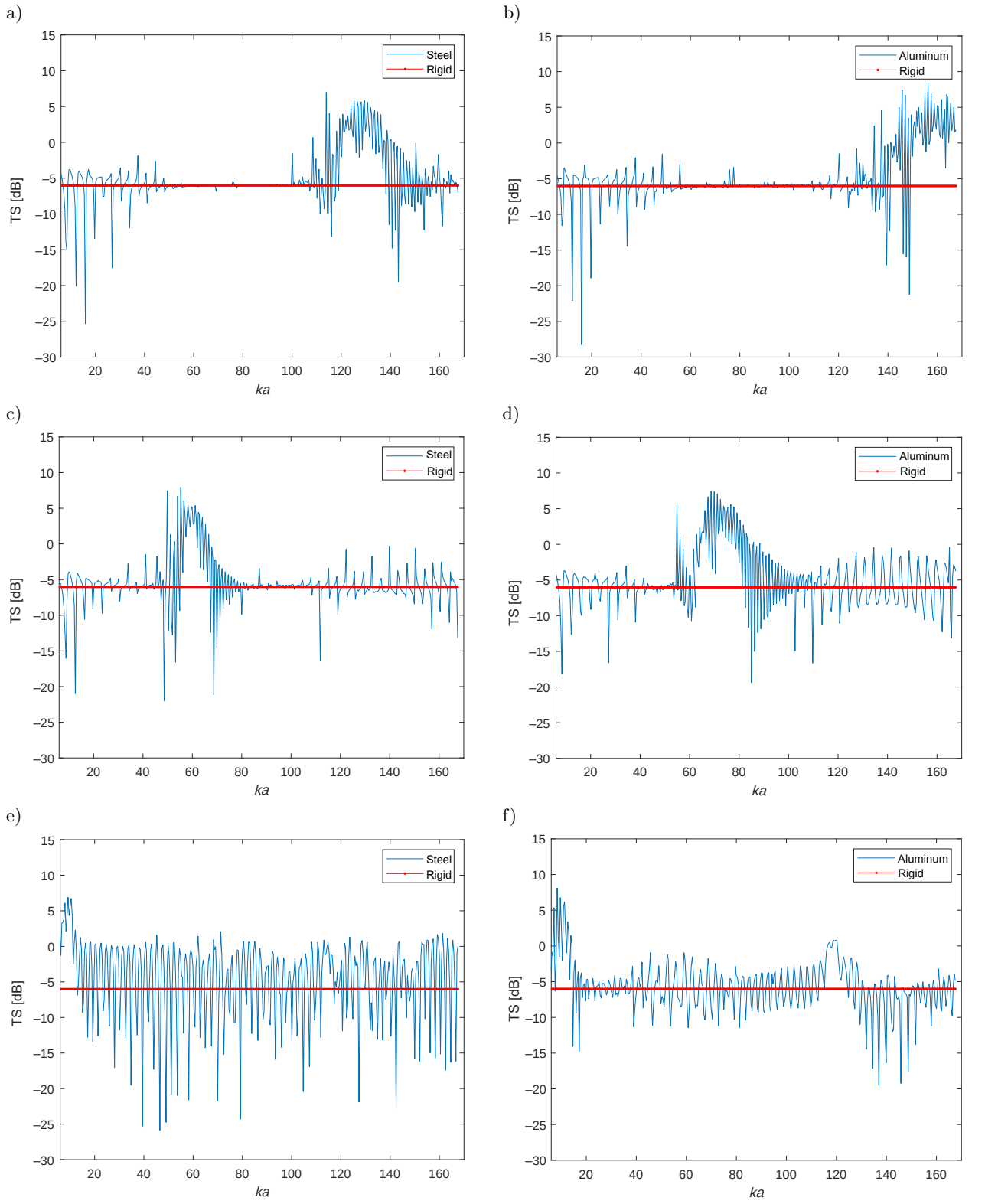

Fig. 7. Calculations of TS of spherical shells with different thickness to radius ratios: a) steel shell and the ratio is 1%; b) aluminum shell and the ratio is 1%; c) steel shell and the ratio is 2%; d) aluminum shell and the ratio is 2%; e) steel shell and the ratio is 10%; f) aluminum shell and the ratio is 10%.

middle-frequency enhancement of different materials are different under the same thickness of the spherical shell. When the steel spherical shell is strengthened, its *ka* value is slightly smaller than that of the aluminum spherical shell. Therefore, when designing a solid-filled spherical shell with specific requirements

for frequency applicability, to reduce the volume of the spherical shell, steel materials can be used for low-frequency spherical shells, and a spherical shell suitable for high-frequency can be made of aluminum.

4.2. Analysis and selection of solid materials filled in the spherical shell

The fourth layer of the solid-filled spherical shell is a solid sphere. The acoustic properties of the solid sphere's materials have a strong influence on the TS of the overall spherical shell. Therefore, it is necessary to discuss the acoustic scattering capabilities of solid spheres made of different materials. We note that research on focusing spheres filled with liquid has been relatively mature (Jia *et al.*, 2020). One of the important conditions for selecting the fourth layer's solid sphere material is the slow propagation speed of sound waves in the solid material. In addition, to conveniently place solid-filled spherical shells in water, the density of the inner spherical solid filler should be as close as possible to the density of the water. According to the relevant literature, an RTV rubber material meets the above requirements (Niu, Zhang, 1982). The specific parameters are as follows: SDL-1-41 material, density 1031 kg/m^3, longitudinal wave velocity 1030 m/s, and transverse wave velocity 201.98 m/s. Of course, other alternative materials can also be used if the sound speed and density conditions are met.

In summary, the inner solid sphere materials discussed in this paper are steel, aluminum, and RTV materials with low sound velocity characteristics. The results are compared with the rigid sphere's TS of the same radius. The material parameter settings are shown in Table 1. The other calculation conditions are as follows: the radius of the spherical shell is 1 m and the medium outside the spherical shell is water.

Figure 8 shows that the TS of the steel sphere and aluminum sphere fluctuates near the theoretical value of the rigid sphere, while the TS of the RTV sphere

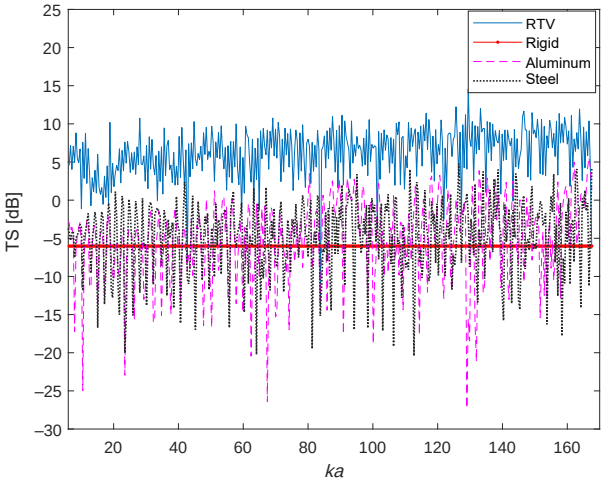

Fig. 8. TS of solid spheres with different materials.

is significantly higher than that of the remaining three spheres. Compared with the theoretical value of the rigid sphere, the TS of the RTV solid sphere is 6–16 dB higher, and the acoustic enhancement effect is obvious. Therefore, during the design of the spherical shell filled with a solid, if we want to improve its TS, the inner solid sphere can be made of RTV material.

4.3. Selection and analysis of the materials of the middle layer

The coupling (middle) layer is a layer of fluid (liquid or air) positioned between the inner solid sphere and the outer spherical shell. The selection of the coupling layer material and the design of its thickness will have a certain impact on the TS of the solid-filled spherical shell. In this paper, air or water is used as the coupling layer material, and the influence of the coupling layer thickness on the TS is discussed.

Calculation condition 1: the spherical shell is made of steel with a radius of 1 m, the thickness of the spherical shell is 1% of the radius (thin spherical shell), the solid sphere material is RTV, the middle coupling layer material is air or water, the radius of the inner solid sphere is 0.5–0.99 m, the corresponding coupling layer thickness is 0.49–0 m, and the other material properties are listed in Table 1.

Figure 9a shows that when the material of the middle coupling layer of the thin spherical shell is water, the thickness of the coupling layer gradually decreases with the increase in the radius of the inner solid sphere between 0.5 m and 0.99 m, and the TS of the solid-filled spherical shell fluctuates but increases overall. When the radius of the solid sphere is 0.99 m, the thickness of the coupling layer is close to 0, that is, the inner solid sphere is close to the spherical shell. When the value of ka is large, the TS has a maximum value of approximately 20 dB, which is 26 dB higher than the TS (−6 dB) of a rigid sphere with the same radius.

Figure 9b reveals that when the medium of the middle coupling layer of a thin spherical shell is air, as the acoustic impedance of air and water has a large difference and acoustic waves are approximately totally reflected, the TS, in this case, is similar to that of a rigid sphere (−6 dB under calculation conditions). However, with increasing frequency, the thin spherical shell in calculation condition 1 gradually gains the characteristics of a thick spherical shell. Therefore, at high frequency, its TS is higher than that of a rigid sphere with the same radius.

Calculation condition 2: the spherical shell is made of steel with a radius of 1 m, the thickness of the spherical shell is 10% of the radius (so we have a thick spherical shell), the inner solid sphere material is RTV, the middle coupling layer material is air or water, the inner solid sphere's radius is 0.5–0.9 m, and the cor-

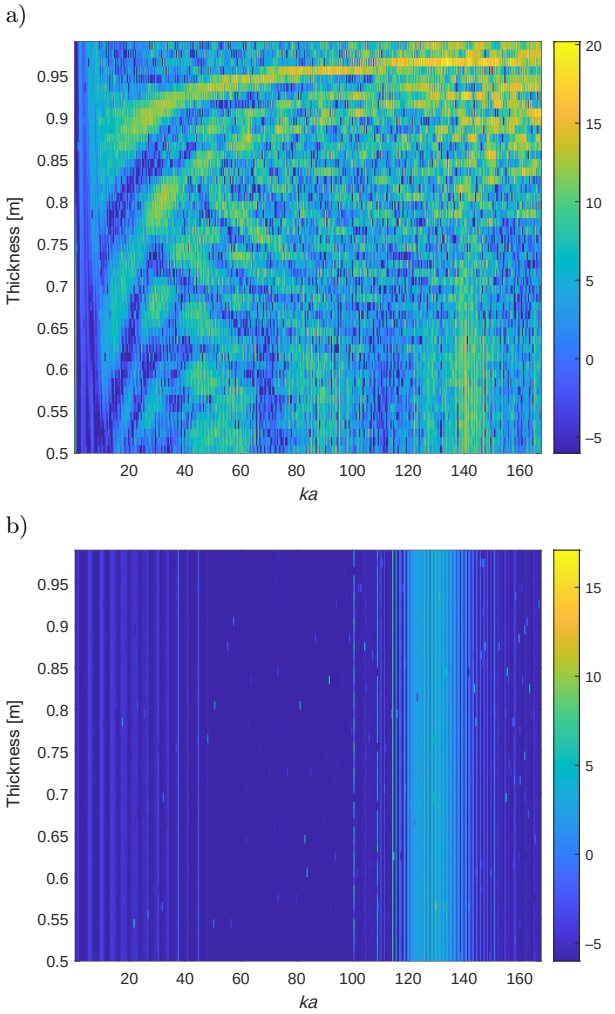

Fig. 9. Calculation of TS of a thin shell sphere changing with coupling layer thickness: a) water filling; b) air filling.

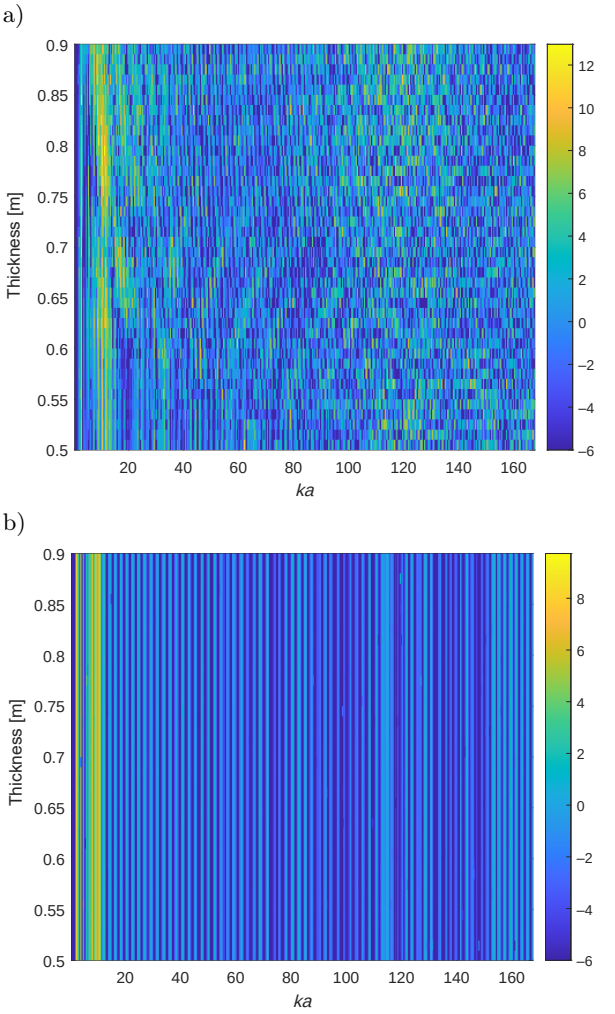

Fig. 10. Calculation of TS of a thick shell sphere changing with coupling layer thickness: a) water filling; b) air filling.

responding middle coupling layer thickness is 0.4–0 m. Other material properties are given in Table 1.

Figure 10a shows that when the medium of the middle coupling layer of the thick spherical shell is water, there is an obvious peak near the low-frequency band (ka = 10) due to the thickness of the outer shell, and the TS is greater than 12 dB. Due to the influence of the middle coupling layer and inner solid sphere, the TS of the solid-filled spherical shell has strong and weak periodic variations.

Figure 10b shows that when the medium of the middle coupling layer of the thick spherical shell is air, similar to Fig. 10a, there is a stable and obvious peak near the low-frequency band, and the TS is approximately 10 dB. Due to the poor coupling effect of air, the influence of solid-filled spheres in the inner layer is almost not reflected, resulting in the same change in the TS with ka for all thicknesses, as shown in the figure.

To better compare the influence of different materials as coupling layer materials on the TS of solid-filled spherical shells, the TS calculation results of these shells with different coupling layer materials under the same conditions are selected for comparison. In the calculation, the material of the spherical shell is steel, the radius is 1 m, the shell thickness is 0.05 m, the inner solid sphere's material is RTV, the middle coupling layer material is air or water, the inner solid sphere radius is 0.9 m, and other material properties are given in Table 1.

In summary, the fourth layer solid sphere plays a major role in enhancing the TS. The strengthening effect of the outer-thickness spherical shell is weaker than that of the inner-filled sphere. The TS strengthening effect of the outer-layer-thickness spherical shell has a certain frequency selectivity. When the middle layer is water, the coupling effect is good (Fig. 11), enabling the full utilization of the TS enhancement effect of the inner solid sphere. When the middle layer is gas, the coupling effect is poor, and the enhancement effect of the inner solid sphere cannot be realized. Therefore, when a high TS is needed, the middle coupling layer uses water. Of course, other liquids can also be used. However, the use of water as a coupling material

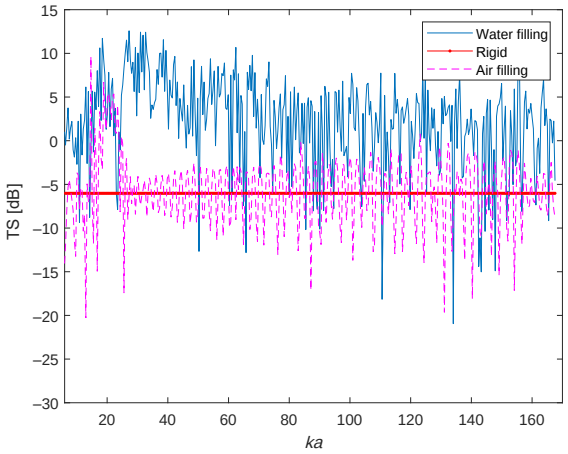

Fig. 11. Comparison of TS of solid-filled spheres with different coupling materials.

has another advantage: the shell structure can be designed to allow water penetration to reduce the weight of solid-filled spherical shells resulting from their closed design, and this, in turn, facilitates the implementation of offshore tests.

5. Conclusions

The normal mode solution of the scattering sound field from a solid-filled spherical shell derived in this paper is in good agreement with the finite element numerical solution, which proves that the solution can be used to calculate the sound scattering characteristics of solid-filled spherical shells.

The sound scatterer of the spherical shell-water-RTV structure has the underwater acoustic focusing ability, which can improve the TS.

Due to the frequency-selective enhancement characteristics of spherical shells with different thicknesses, when designing underwater acoustic standards and markers, the thicknesses of spherical shells can be designed to match the working frequency band of the available underwater acoustic equipment.

Appendix

Solution of the scattering coefficient b_n of the solid-filled spherical shell.

$$b_n = -\frac{B_n}{D_n},$$

$$B_n = \begin{vmatrix} A_1 & d_{12} & d_{13} & d_{14} & d_{15} & d_{16} & d_{17} & d_{18} & d_{19} \\ A_2 & d_{22} & d_{23} & d_{24} & d_{25} & d_{26} & d_{27} & d_{28} & d_{29} \\ d_{31} & d_{32} & d_{33} & d_{34} & d_{35} & d_{36} & d_{37} & d_{38} & d_{39} \\ d_{41} & d_{42} & d_{43} & d_{44} & d_{45} & d_{46} & d_{47} & d_{48} & d_{49} \\ d_{51} & d_{52} & d_{53} & d_{54} & d_{55} & d_{56} & d_{57} & d_{58} & d_{59} \\ d_{61} & d_{62} & d_{63} & d_{64} & d_{65} & d_{66} & d_{67} & d_{68} & d_{69} \\ d_{71} & d_{72} & d_{73} & d_{74} & d_{75} & d_{76} & d_{77} & d_{78} & d_{79} \\ d_{81} & d_{82} & d_{83} & d_{84} & d_{85} & d_{86} & d_{87} & d_{88} & d_{89} \\ d_{91} & d_{92} & d_{93} & d_{94} & d_{95} & d_{96} & d_{97} & d_{98} & d_{99} \end{vmatrix},$$

$$D_n = \begin{vmatrix} d_{11} & d_{12} & d_{13} & d_{14} & d_{15} & d_{16} & d_{17} & d_{18} & d_{19} \\ d_{21} & d_{22} & d_{23} & d_{24} & d_{25} & d_{26} & d_{27} & d_{28} & d_{29} \\ d_{31} & d_{32} & d_{33} & d_{34} & d_{35} & d_{36} & d_{37} & d_{38} & d_{39} \\ d_{41} & d_{42} & d_{43} & d_{44} & d_{45} & d_{46} & d_{47} & d_{48} & d_{49} \\ d_{51} & d_{52} & d_{53} & d_{54} & d_{55} & d_{56} & d_{57} & d_{58} & d_{59} \\ d_{61} & d_{62} & d_{63} & d_{64} & d_{65} & d_{66} & d_{67} & d_{68} & d_{69} \\ d_{71} & d_{72} & d_{73} & d_{74} & d_{75} & d_{76} & d_{77} & d_{78} & d_{79} \\ d_{81} & d_{82} & d_{83} & d_{84} & d_{85} & d_{86} & d_{87} & d_{88} & d_{89} \\ d_{91} & d_{92} & d_{93} & d_{94} & d_{95} & d_{96} & d_{97} & d_{98} & d_{99} \end{vmatrix},$$

where

$$d_{11} = (\rho_1/\rho_2)k_{s2}^2 a^2 h_n^{(1)}(k_1 a),$$

$$d_{12} = \left[2n\,(n+1) - k_{s2}^2 a^2\right] j_n\,(k_{d2}a) - 4k_{d2}a j_n'(k_{d2}a),$$

$$d_{13} = \left[2n\,(n+1) - k_{s2}^2 a^2\right] y_n\,(k_{d2}a) - 4k_{d2}a y_n'(k_{d2}a),$$

$$d_{14} = 2n(n+1)\left[k_{s2}a j_n'\,(k_{s2}a) - j_n(k_{s2}a)\right],$$

$$d_{15} = 2n(n+1)\left[k_{s2}a y_n'\,(k_{s2}a) - y_n(k_{s2}a)\right],$$

$$d_{16} = 0,$$

$$d_{17} = 0,$$

$$d_{18} = 0,$$

$$d_{19} = 0,$$

$$d_{21} = -k_1 a h_n^{(1)'}(k_1 a),$$

$$d_{22} = k_{d2}a j_n'\,(k_{d2}a)\,,$$

$$d_{23} = k_{d2}a y_n'\,(k_{d2}a)\,,$$

$$d_{24} = n(n+1) j_n\,(k_{s2}a)\,,$$

$$d_{25} = n(n+1) y_n\,(k_{s2}a)\,,$$

$$d_{26} = 0,$$

$$d_{27} = 0,$$

$$d_{28} = 0,$$

$$d_{29} = 0,$$

$$d_{31} = 0,$$

$$d_{32} = 2\left[j_n(k_{d2}a) - k_{d2}a j_n'(k_{d2}a)\right],$$

$$d_{33} = 2\left[y_n(k_{d2}a) - k_{d2}a y_n'(k_{d2}a)\right],$$

$$d_{34} = 2k_{s2}a j_n'(k_{s2}a) + \left[(k_{s2}a)^2 - 2n(n+1) + 2\right] j_n(k_{s2}a),$$

$$d_{35} = 2k_{s2}a y_n'(k_{s2}a) + \left[(k_{s2}a)^2 - 2n(n+1) + 2\right] y_n(k_{s2}a),$$

$$d_{36} = 0,$$

$$d_{37} = 0,$$

$$d_{38} = 0,$$

$$d_{39} = 0,$$

$$d_{41} = 0,$$

$$d_{42} = \left[2n(n+1) - (k_{s2}b)^2\right] j_n(k_{d2}b) - 4k_{d2}bj'_n(k_{d2}b),$$

$$d_{43} = \left[2n(n+1) - (k_{s2}b)^2\right] y_n(k_{d2}b) - 4k_{d2}by'_n(k_{d2}b),$$

$$d_{44} = 2n(n+1)\left[k_{s2}bj'_n(k_{s2}b) - j_n(k_{s2}b)\right],$$

$$d_{45} = 2n(n+1)\left[k_{s2}by'_n(k_{s2}b) - y_n(k_{s2}b)\right],$$

$$d_{46} = (\rho_3/\rho_2)(k_{s2}b)^2 j_n(k_3b),$$

$$d_{47} = (\rho_3/\rho_2)(k_{s2}b)^2 y_n(k_3b),$$

$$d_{48} = 0,$$

$$d_{49} = 0,$$

$$d_{51} = 0,$$

$$d_{52} = k_{d2}bj'_n(k_{d2}b),$$

$$d_{53} = k_{d2}by'_n(k_{d2}b),$$

$$d_{54} = n(n+1)j_n(k_{s2}b),$$

$$d_{55} = n(n+1)y_n(k_{s2}b),$$

$$d_{56} = -k_3bj'_n(k_3b),$$

$$d_{57} = -k_3by'_n(k_3b),$$

$$d_{58} = 0,$$

$$d_{59} = 0,$$

$$d_{61} = 0,$$

$$d_{62} = 2\left[j_n(k_{d2}b) - k_{d2}bj'_n(k_{d2}b)\right],$$

$$d_{63} = 2\left[y_n(k_{d2}b) - k_{d2}by'_n(k_{d2}b)\right],$$

$$d_{64} = 2k_{s2}bj'_n(k_{s2}b) + \left[(k_{s2}b)^2 - 2n(n+1)+2\right] j_n(k_{s2}b),$$

$$d_{65} = 2k_{s2}by'_n(k_{s2}b) + \left[(k_{s2}b)^2 - 2n(n+1)+2\right] y_n(k_{s2}b),$$

$$d_{66} = 0,$$

$$d_{67} = 0,$$

$$d_{68} = 0,$$

$$d_{69} = 0,$$

$$d_{71} = 0,$$

$$d_{72} = 0,$$

$$d_{73} = 0,$$

$$d_{74} = 0,$$

$$d_{75} = 0,$$

$$d_{76} = (\rho_3/\rho_4)(k_{s4}R_1)^2 j_n(k_3R_1),$$

$$d_{77} = (\rho_3/\rho_4)(k_{s4}R_1)^2 y_n(k_3R_1),$$

$$d_{78} = \left[2n\,(n+1) - (k_{s4}R_1)^2\right] j_n\,(k_{d4}R_1) - 4k_{d4}R_1j'_n(k_{d4}R_1),$$

$$d_{79} = 2n(n+1)\left[k_{s4}R_1j'_n\,(k_{s4}R_1) - j_n(k_{s4}R_1)\right],$$

$$d_{81} = 0,$$

$$d_{82} = 0,$$

$$d_{83} = 0,$$

$$d_{84} = 0,$$

$$d_{85} = 0,$$

$$d_{86} = -k_3R_1j'_n(k_3R_1),$$

$$d_{87} = -k_3R_1y'_n(k_3R_1),$$

$$d_{88} = k_{d4}R_1j'_n(k_{d4}R_1),$$

$$d_{89} = n(n+1)j_n(k_{s4}R_1),$$

$$d_{91} = 0,$$

$$d_{92} = 0,$$

$$d_{93} = 0,$$

$$d_{94} = 0,$$

$$d_{95} = 0,$$

$$d_{96} = 0,$$

$$d_{97} = 0,$$

$$d_{98} = 2\left[j_n(k_{d4}R_1) - k_{d4}R_1j'_n(k_{d4}R_1)\right],$$

$$d_{99} = 2k_{s4}R_1j'_n(k_{s4}R_1) + \left[(k_{s4}R_1)^2 - 2n(n+1) + 2\right] j_n(k_{s4}R_1),$$

$$A_1 = (\rho_1/\rho_2)(k_{s2}a)^2 j_n(k_1a),$$

$$A_2 = -k_1aj'_n(k_1a),$$

where ρ_1 is the density of (1) layer, $j'_n(X)$ is the derivative of the n-th-order Bessel function, $y'_n(X)$ is the derivative of the n-th-order Neumann function, and $h_n^{(1)'}(X)$ is the derivative of the n-th-order Hankel function of the first kind.

Acknowledgments

This research was supported by the National Natural Science Foundation of China (grant no. 61901079).

References

1. Anstee S. (2002), *Use of spherical objects as calibrated mine hunting sonar targets*, Maritime Operations Division Systems Sciences Laboratory, DSTO-TN-0425.
2. Atkins P.R., Yan T., Hayati F. (2017), Standard target calibration: practical intercomparison with planar surface targets and calibrated transducers, [in:] *Proceeding of Oceans '17 MTS/IEEE*, doi: 10.1109/OCEANSE.2017.8084801.
3. Deng W.-X., Yang T.-S., Yang J.-B. (1982), Experimental study on liquid filled focused spherical reflector [in Chinese], *Acta Acustica*, **7**(2): 88–93, doi: 10.15949/j.cnki.0371-0025.1982.02.003.
4. Deveau D.M., Lyons A.P. (2009), Fluid-filled passive sonar calibration spheres: Design, modeling, and measurement, *IEEE Journal of Oceanic Engineering*, **34**(1): 93–100, doi: 10.1109/JOE.2008.2010755.
5. Fan J., Tang W.L. (2001), Echoes from double elastic spherical shell covered with viscoelastic materials in water [in Chinese], *Acta Acustica*, **26**(4): 302–306, doi: 10.15949/j.cnki.0371-0025.2001.04.003.
6. Fawcett J.A. (2001), Scattering from a partially fluid-filled, elastic shelled sphere, *The Journal of the Acoustical Society of America*, **109**(2): 508–513, doi: 10.1121/1.1339827.
7. Foote K.G. (2018), Standard-target calibration of active sonars used to measure scattering: principles and illustrative protocols, *IEEE Journal of Oceanic Engineering*, **43**(3): 749–763, doi: 10.1109/JOE.2017.2713538.
8. Foote K.G., Francis D.T.I., Atkins P.R. (2007), Calibration sphere for low-frequency parametric sonars, *The Journal of the Acoustical Society of America*, **121**(3): 1482–1490, doi: 10.1121/1.2434244.
9. Goodman R.R., Stern R. (1962), Reflection and transmission of sound by elastic spherical shells, *Journal of the Acoustical Society of America*, **34**(3): 338–344, doi: 10.1121/1.1928120.
10. Islas-Cital A., Atkins P. (2012), Practical consideration in the amplitude and phase calibration of SONAR systems in laboratory water tanks using the standard-target method, [in:] *Proceedings of Meetings on Acoustics, ECUA 2012 11th European Conference on Underwater Acoustics*, **17**(1): 070013, doi: 10.1121/1.4767969.
11. Jia B., Wang J.H., Li G.J., Chen Y.F. (2020), Numerical analysis on target strength of the filled spherical elastic shell, *IOP Conference Series: Materials Science and Engineering*, **813**: 012004, doi: 10.1088/1757-899X/813/1/012004.
12. Junger M.C. (1952), Sound scattering by thin elastic shells, *The Journal of the Acoustical Society of America*, **24**(4): 336–373, doi: 10.1121/1.1906905.
13. Kaduchak G., Loeffler C.M. (1998), Relationship between material parameters and target strength of fluid-filled spherical shells in water: Calculations and observations, *IEEE Journal of Oceanic Engineering*, **23**(1): 26–30, doi: 10.1109/48.659447.
14. Niu F.Q., Zhang X.P. (1982), Acoustic properties of domestic RTV silicone rubber [in Chinese], *Applied Acoustics*, **1**(4): 39–42.
15. Stanton T.K., Chu D. (2008), Calibration of broadband active acoustic systems using a single standard spherical target, *The Journal of the Acoustical Society of America*, **124**(1): 128–136, doi: 10.1121/1.2917387.
16. Tang W.L., Fan J. (1999), Echoes from double elastic spherical shell in water [in Chinese], *Acta Acustica*, **24**(2): 174–182, doi: 10.15949/j.cnki.0371-0025.1999.02.009.
17. Tang W.L., Fan J., Ma Z.C. (2018), *Acoustic Scattering from Underwater Targets*, Science Press.
18. Xu S.Y., Fan J., Wang B. (2020), Low frequency target strength enhancement based on acoustic tunnel effect, *Technical Acoustics*, **39**(1): 34–39, doi: 10.16300/j.cnki.1000-3630.2020.01.006.
19. Zhou Y.L., Fan J., Wang B. (2019), Inversion for acoustic parameters of plastic polymer target in water [in Chinese], *Acta Physica Sinica*, **68**(21): 214301, doi: 10.7498/aps.68.20190991.
20. Zhou Y.L., Fan J., Wang B. (2020), Phase characteristics of acoustic-scattering field for underwater spherical targets [in Chinese], *Journal of Harbin Engineering University*, **41**(7): 945–950, doi: 10.11990/jheu.201905022.